RSC Advances

ROYAL SOCIETY OF CHEMISTRY

www.rsc.org/advances

ARTICLE TYPE www.rsc.org/xxxxxx | XXXXXXXX

A Quenching Method for the Preparation of Metal Oxide/Polythiophene Composites Having Fiber Structures

Fang-Hsien Lu[a], Mohamed-Gamal Mohamed[b], Tzeng-Feng Liu[a], Chuen-Guang Chao[a], Lizong Dai[c], and Shiao-Wei, Kuo[b,*]

Received (in XXX, XXX) Xth XXXXXXXXX 200X, Accepted Xth XXXXXXXXX 200X
First published on the web Xth XXXXXXXXX 200X
DOI: 10.1039/b000000x

In this study we developed a simple quenching method to fabricate metal oxide (CuO, ZnO, TiO_2, $Fe(OH)_3$)/polythiophene (PT) composites; by varying the metal oxide, PT, and rate of crystallization, we could control the fiber morphology in these composites. Four-probe-station analyses revealed that the conductivities of these metal oxide/PT composites ranged from 10^{-5} to 10^{-3} S/cm, higher than those of any species of metal oxide alone (from 10^{-10} to 10^{-7} S/cm), because the fiber morphology behaved as an exceptional transmission factor for electrons. Moreover, these metal oxide/PT composites exhibited the characteristics of colloids, as well as high viscosity, suggesting that they could also be applied as coatings on silicon and glass substrates, and these were most opportunity to form in the useful material for large-scale gas-sensor due to well flexibility and porosity. UV–Vis spectroscopic analyses revealed variations in the energy level (>3.37 eV as ZnO) and confirmed the mechanism of the composite morphology change.

Introduction

Many fabrication methods, including vapor–liquid–solid (VLS), metal–organic chemical vapor deposition, physical vapor deposition (PVD), and microwave hydrothermal methods, can be employed to produce narrow materials for application in nanotechnology. For example, ZnO nanowire[1] and nanorod arrays are often prepared using the VLS method; even through this method is restricted by the need for high temperatures. Similarly, ZnO nanosheet and branch structures can be obtained through the PVD method, which also requires stringent conditions (e.g., high vacuum)[2]. Likewise, hydrothermal[3-6] and laser ablation[7-10] methods can be performed only under severe conditions.

Accordingly, industrial and academic researchers are seeking new facile methods for the preparation of nanomaterials at relatively low cost. Fabrication involving many kinds of nanostructures, including nanodendrites,[11-13] can be accomplished inexpensively using, for example, chemical solutions,[14-16] solvothermal reactions,[17,18] and water baths. In this present study, we developed a new technique, a so-called "quenching method," for manufacturing metal oxide/polymer fibers. This quenching method involves setting the precipitation properties of the metallic and ceramic materials at low temperatures and controlling the nucleation rate[19–21] and the growth orientation[22–24] of the nanostructures. Noble metal nanoparticles of uniform size can be fabricated through a drastic variation of temperature in a microwave hydrothermal procedure as the result of a rapid rate of nucleation among the metal atoms. Moreover, a slow rate of crystallization can occur at low temperatures, leading to the formation of rod structures with a fixed growth orientation.

Among the various nanostructures, fiber structures are interesting research materials because they possess large aspect ratios, resulting in large specific surface areas, high activities, and good growth orientation. The conditions for controlled growth of fiber structures can, however, involve exposure to severe environments. A quenching method could, therefore, become a profitable means of fabricating fiber structures. Because high affinity exists between metal cations and thioethers, which are subunits of polythiophene (PT) structures, such polymers can bind to metal cations and affect their stacking when fabricating metallic compound/polymer fiber structures. We suspected that such fiber structures might improve the efficiency of photoelectric devices. Hence, in the present study we used this quenching method to manufacture composite materials, exhibiting high conductivity and high elasticity, for use in improving capacitance and applications in electrodes of solar cells and gas sensors. Moreover, the fiber structure including well flexibility, tensile strength modules, and porosity can be advanced the adsorption ability and detection limit of large scale gas sensor. Even the preparations of the transporting layers of solar cell are simplified by metallic compound/polymer composites with viscosity and coating property.

Experimental

Materials

$FeCl_3$ (assay: ≥99.99% trace metal basis; M_p: 304 °C), $CuCl_2$ (assay: ≥99.995% trace metal basis; M_p: 620 °C; d = 3.38 g/cm^3, at 25 °C), $ZnCl_2$ (assay: ≥99.995% trace metal basis; M_p: 293 °C; B_p: 732 °C/1 atm), $TiCl_3$ (assay: ≥99.995% trace metal basis; M_p: 440 °C), thiophene (C_4H_4S; assay: ≥99%; B_p: 84 °C), poly(vinyl alcohol) [$(C_2H_4O)_n$; molecular weight: 89,000–98,000 g/mol), and NaOH (assay: ≥98%; total impurities: ≤1.0% Na_2CO_3), were purchased from Sigma–Aldrich. Ethylene glycol [$C_2H_4(OH)_2$; M_p: –13 °C; B_p: 194 °C; d = 1.11 g/cm^3) was obtained from J. T. Baker.

Metal oxide/polymer complexes

A fixed quantity of a metal chloride powder was dissolved in ethylene glycol to prepare a solution having a concentration of 32,000 ppm. This solution was mixed with 3 wt% poly(vinyl alcohol) and stirred at 70 °C for 1 h. Thiophene [6.4 g (0.076 mol), 9.6 g (0.114 mol), or 12.8 g (0.152 mol)] was injected via

[a]Department of Materials Science and Engineering, National Chiao Tung University, Hsinchu 300, Taiwan
[b]Department of Materials and Optoelectronic Science, Center for Functional Polymers and Supramolecular Materials, National Sun Yat-Sen University, Kaohsiung, 804, Taiwan.
E-mail: kuosw@faculty.nsysu.edu.tw
[c]Department of Material Science and Engineering, Fujian Provincial Key Laboratory of Fire Retardant Materials, College of Materials, Xiamen University, Xiamen Fujian, China.

syringe. The mixture was stirred continuously at 70 °C for 1 h

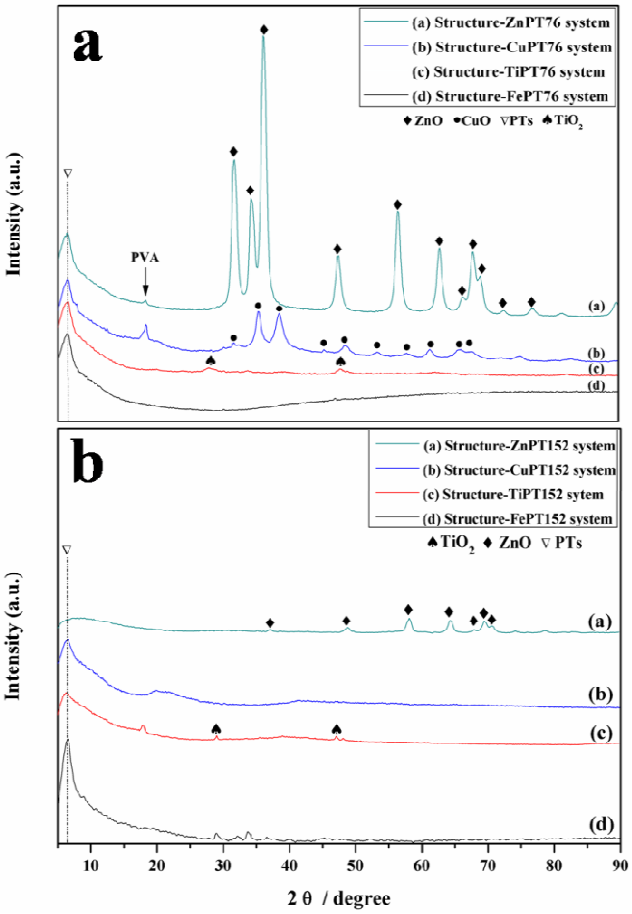

Figure 1: XRD patterns of the products fabricated from the (a) MPT76 and (b) MPT152 systems.

before cooling rapidly to –40 °C in a liquid-nitrate mixed system. 3 M NaOH was added slowly to the mixture. A metal hydroxide—brown $Fe(OH)_3$, blue $Cu(OH)_2$, or white $Zn(OH)_2$—precipitated rapidly. The mixtures were maintained at –40 °C for period of time to completely convert the metal chloride to the metal hydroxide. Subsequently, the whole solution, including the precipitate, was stirred at 70 °C for 1 h and then quenched rapidly once again. Finally, the precipitate, corresponding to the product, was washed several times through centrifuging and filtering and was then dried at 65 °C in a precise oven.

Characterization

The structures and compositions of the products were identified through X-ray diffraction (XRD) using a Bruker D8 DISCOVER apparatus; the wavelength (λ) of the incident beam (1.5412 Å) was set using a rotating Cu target. The morphologies and shapes of the nanomaterials were observed through field emission scanning electron microscopy (FE-SEM), using a JSM-7000F microscope (JEOL, Japan), and optical microscopy (OM), using an Olympus BX51-P microscope. The energy levels of the metal oxide/polymer composites were measured through UV–Vis–NIR spectrophotometry (Hitachi U-4100). Electrical properties, including conductivity, were measured through four-probe-station analysis (Hewlett–Packard). Samples for conductivity analysis were prepared in tablet form for comparison with the bulk pure metallic composite.

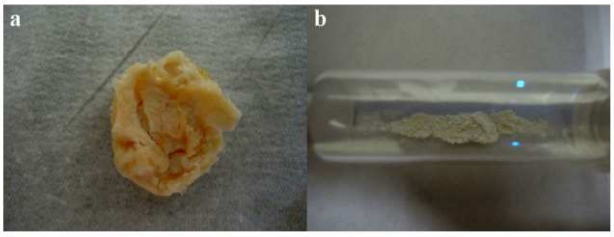

Figure 2: Products fabricated from the ZnPT76 system when using the (a) quenching and (b) hydrothermal methods.

Results and Discussion

Compositions of the products

Figure 1 displays the structures and compositions of the products fabricated from the metal chloride/poly(vinyl alcohol)/thiophene (MPT) systems. The characteristic peak of PT appeared distinctly at a value of 2θ of 2.3–6.3°.[25–27] The presence of ZnO, CuO, and TiO_2 was confirmed by their JCPDS signals; an amorphous phase occurred for $Fe(OH)_3$, however, because of its self-crystalline characteristics. Furthermore, we observed the characteristic crystalline peak of poly(vinyl alcohol) at a value of 2θ of 17–20° in the XRD patterns; the intensity of this peak was weak, however, because poly(vinyl alcohol) functioned as a water-soluble surfactant in our reaction media and was mostly rinsed out from the products. The mechanisms of formation of the metallic compounds presumably occurred as follows:

(a) Formation of CuO

$CuCl_2 + 2NaOH \rightarrow Cu(OH)_2 + 2NaCl$

$Cu(OH)_2 \rightarrow CuO + H_2O$ (heating at 70 °C)

(b) Formation of ZnO

$ZnCl_2 + 2NaOH \rightarrow Zn(OH)_2 + 2NaCl$

$Zn(OH)_2 \rightarrow ZnO + H_2O$ (heating at 70 °C)

(c) Formation of TiO_2

$2TiCl_3 \rightarrow TiCl_2 + TiCl_4$ (in solution)

$TiCl_4 + 2H_2O \rightarrow TiO_2 + 4HCl$

$TiO_2 + 4HCl + 2NaOH \rightarrow TiO_2 + 4H_2O + 4NaCl$

(d) Formation of $Fe(OH)_3$

$FeCl_3 + 3NaOH \rightarrow Fe(OH)_3 + 3NaCl$

$2Fe(OH)_3 \rightarrow Fe_2O_3 + 3H_2O$ (requires heating at 300 °C)

Moreover, the structures of the products were transformed when adding thiophene, as revealed in Figs. 1(a) and 1(b). Figure 1(b) presents the structures fabricated using the metal chloride/poly(vinyl alcohol)/thiophene (0.152 mol) systems (MPT152). The intense signal for the crystallization of the metal oxide weakened in each spectrum, with the trend toward an amorphous structure being most remarkable for the $CuCl_2$/poly(vinyl alcohol)/thiophene (0.152 mole) system (CuPT152). Furthermore, in the ZnPT152 system, most of the strongest peaks were located at higher values of 2θ. These results indicate that the structures of the metal oxides changed from ordered [Fig. 1(a)] to disordered [Fig. 1(b)].

Figure 2 reveals the shapes of the metal oxide/polymer complexes fabricated from the MPT systems using the quenching method. The metal oxide/polymer complexes possessed the elastic properties of colloids before and after drying [Fig. 2(a)]. In contrast, the metal oxide/polymer complexes had powdery properties when fabricated using the hydrothermal method [Fig. 2(b)]. Figures 3 and 4 display OM and SEM images, respectively, of the complexes fabricated from the metal chloride/poly(vinyl alcohol)/thiophene (0.114 mol) systems (MPT114). Each of these complexes possessed the morphology of irregular fibers; such a morphology disappeared, when we fabricated the complex from a

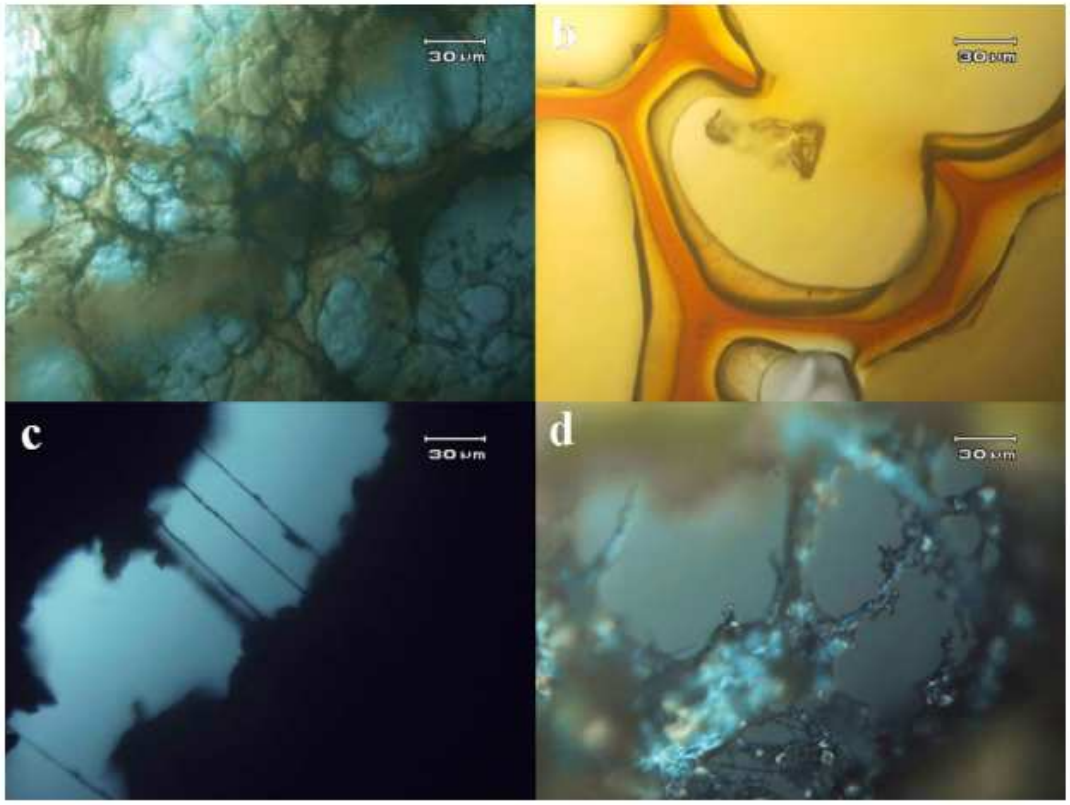

Figure 3: OM images displaying the morphologies of the products fabricated from the MPT114 system: M = (a) Cu, (b) Fe, (c) Zn, and (d) Ti.

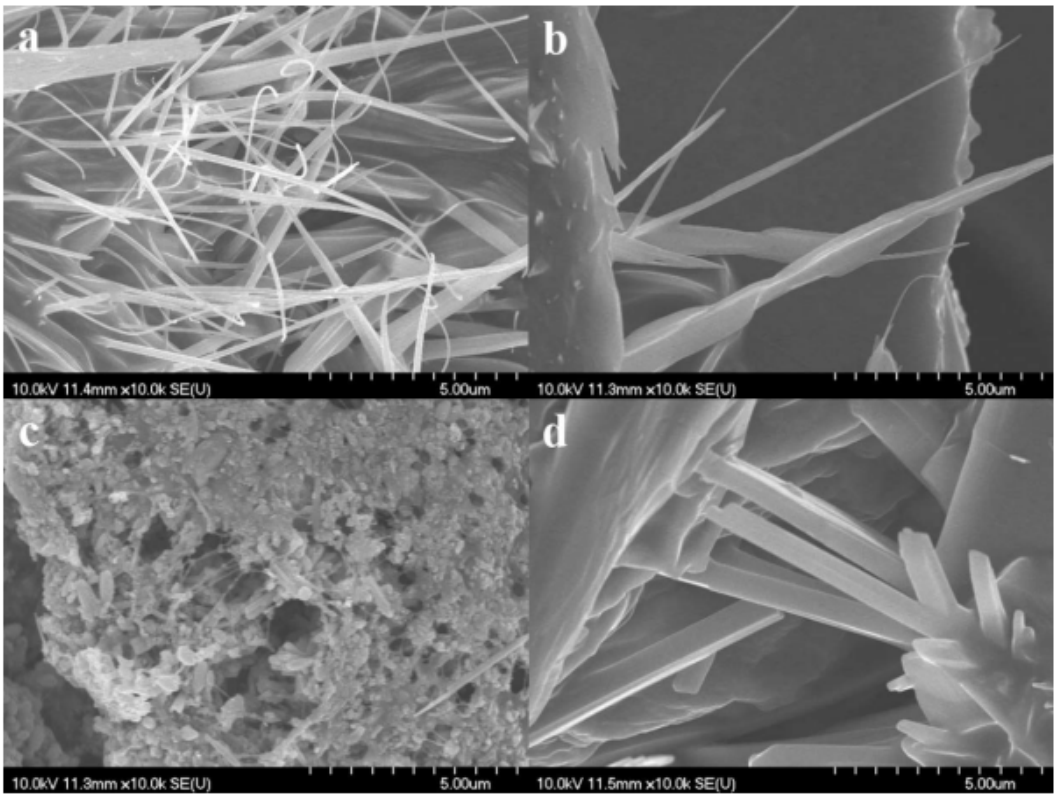

Figure 4: SEM images displaying the morphologies of the products fabricated from the MPT114 system: M = (a) Cu, (b) Fe, (c) Zn, and (d) Ti.

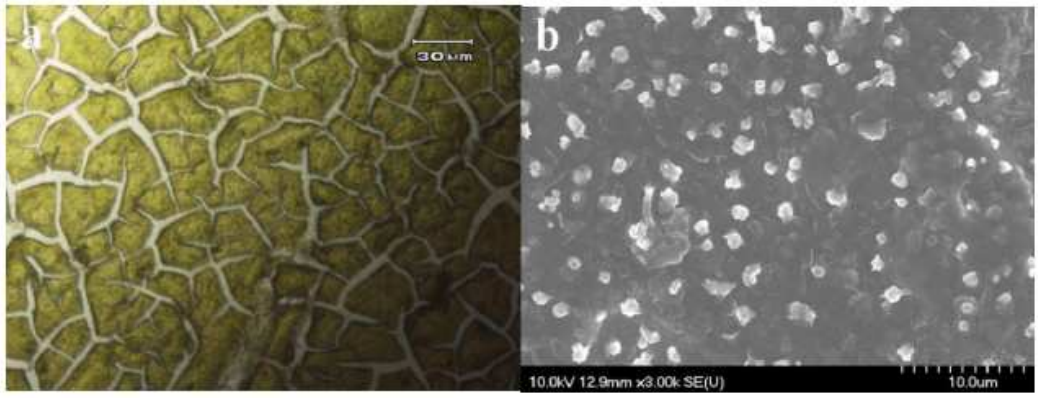

Figure 5: (a) OM and (b) SEM images displaying the morphologies of the products fabricated from the CuP system using the hydrothermal method.

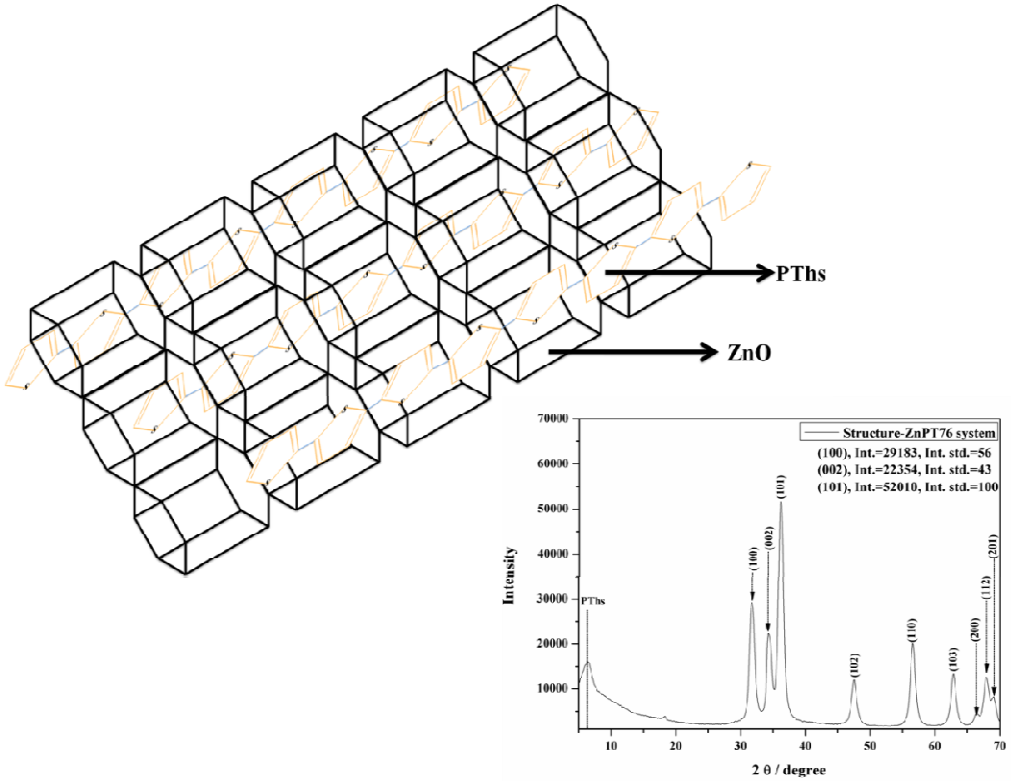

Figure 6: Structures of the products fabricated from the ZnPT76 system.

metal chloride/poly(vinyl alcohol) system (Fig. 5). We suspect that the mechanism of fiber formation occurred as follows. In the MPT system, poly(vinyl alcohol) and ethylene glycol have similar solubility capabilities and can be regarded as surfactants. Polymerization of the thiophene monomers to form PT was mediated by $FeCl_3$ or $CuCl_2$ at low temperature. As mentioned above, these metal cations have affinity for thioether units. Hence, the stacking in the metal oxide lattices was affected by the presence of the PT. After quenching, the low temperature decreased the rates of nucleation and growth. In other words, the lattice of the metal oxide could stack appropriately, with the PTs units in contact with the sides of the metal oxide lattices. Figure 6 illustrates the structure of a fiber; Figure 6 presents the arrangement of the lattices of the metal oxide and the chains of the PT. The hexagonal lattices represent the ZnO crystals; the growth orientation of the fiber structure of the ZnO/PTs complex is indicated in the (101) plane, as determined by comparing the XRD data from this study with those in the JCPDS database.[28,29] In contrast, the PT chains formed irregular and disarranged structures. Hence, the orientation of the metallic composite was not fixed efficiently. The low temperature was another factor that affected the formation of the rods from the metal oxide/polymer complexes. According to the following thermal dynamic functions:

(1) $D^2 - D_0^2 = K_0 e^{-Q/RT}$,

(2) $\log\left(D^2 - \frac{D_0^2}{t}\right) = -\left(\frac{Q}{2.3RT}\right) + \log K_0$,

the driving force for metal oxide nanoparticles and the stacking rate would decrease gradually upon decreasing the temperature. These phenomena would cause the grain sizes of the metallic composites to increase. Thus, micrometer-scale rods would grow from these metallic composites.

OM (Figure 7) revealed the existence and arrangement of the PTs in the complexes. Figures 8 and 9 present SEM images of

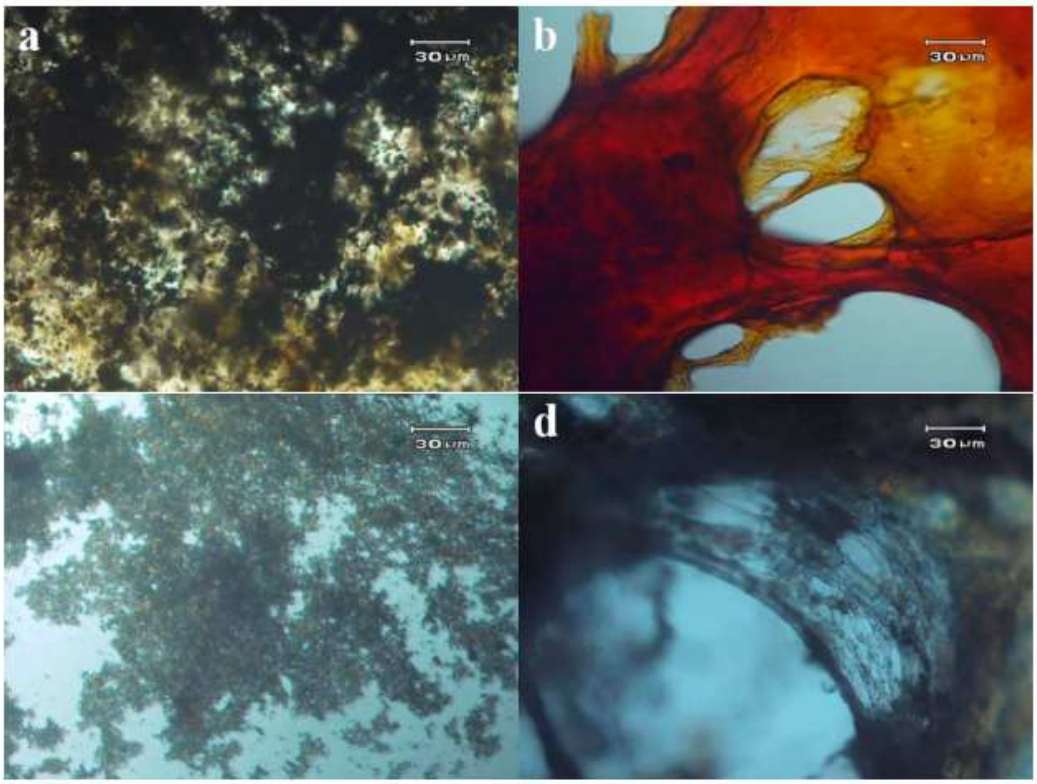

Figure 7: OM images displaying the morphologies of the products fabricated from the MPT76 system: M = (a) Cu, (b) Fe, (c) Zn, and (d) Ti.

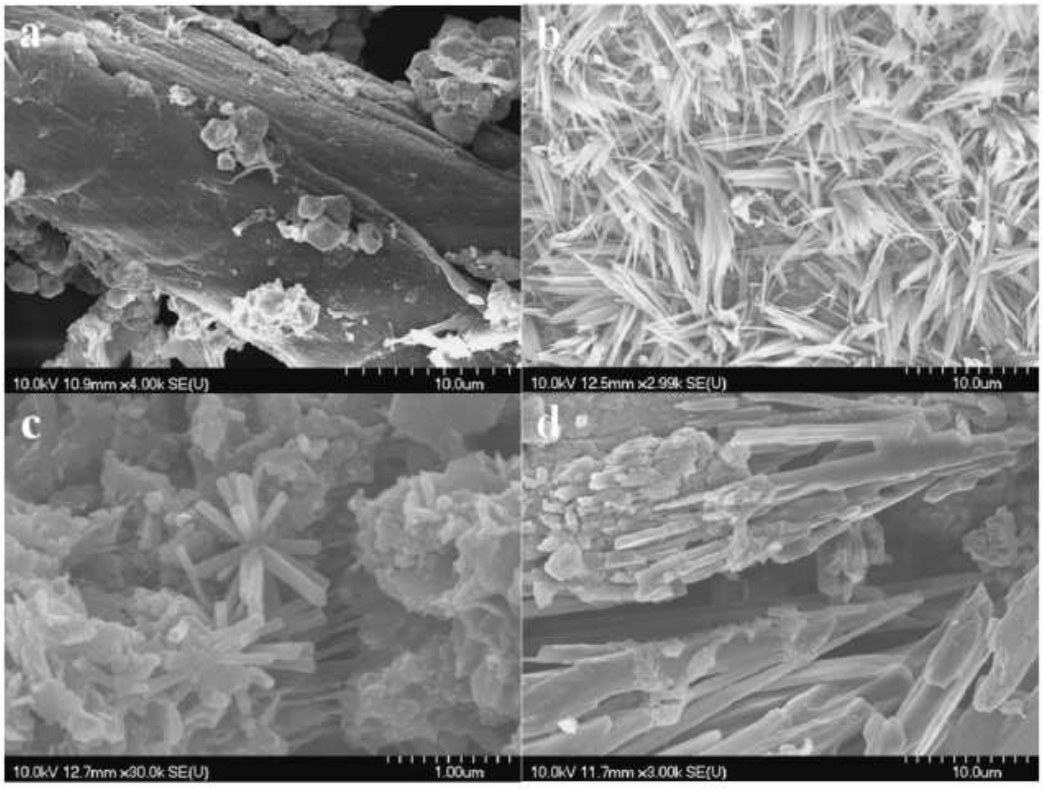

Figure 8: SEM images displaying the morphologies of the products fabricated from the MPT76 system: M = (a) Cu, (b) Fe, (c) Zn, and (d) Ti.

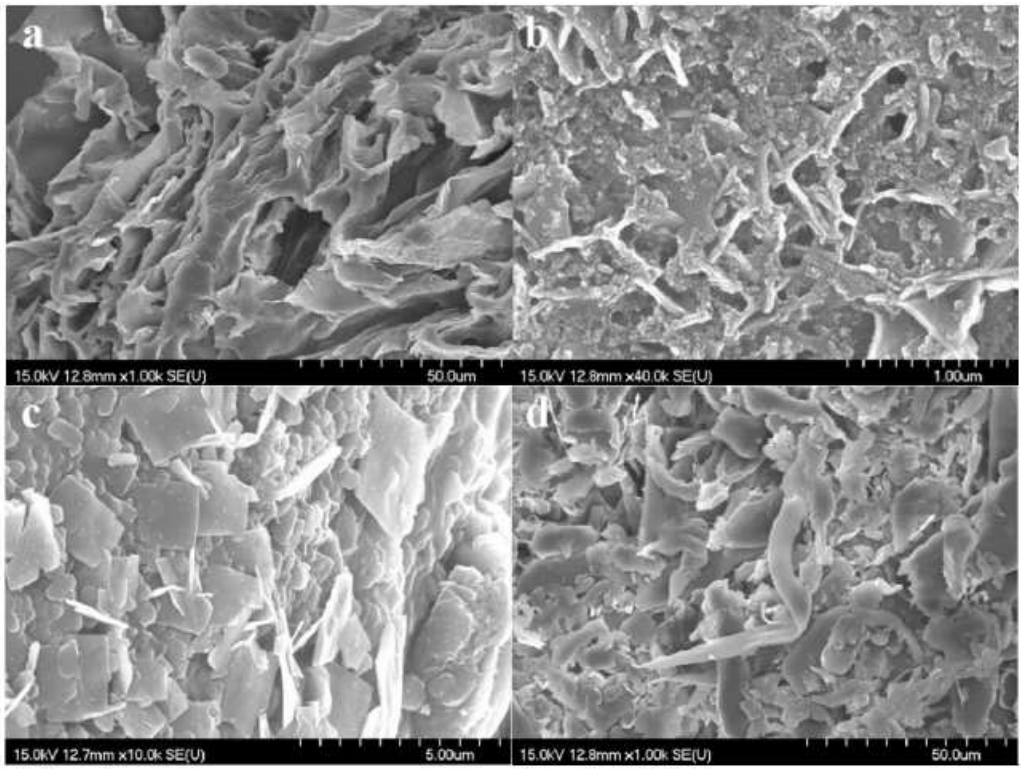

Figure 9: SEM images displaying the morphologies of the products fabricated from the MPT152 system: M = (a) Cu, (b) Fe, (c) Zn, and (d) Ti.

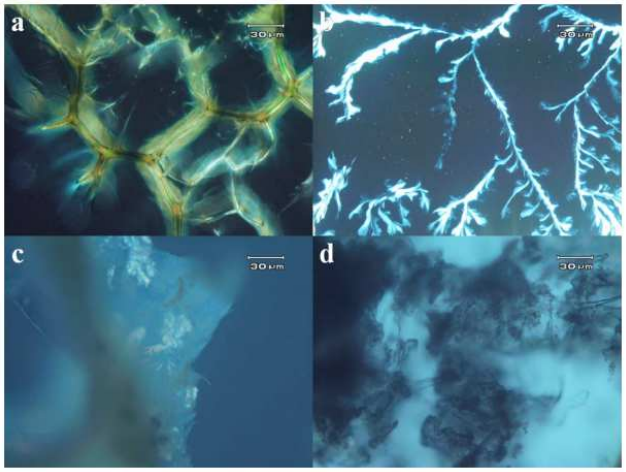

Figure 10: OM images displaying the morphologies of the products fabricated from the MPT152 system: M = (a) Cu, (b) Fe, (c) Zn, and (d) Ti.

the morphologies of the complexes formed from the metal chloride/poly(vinyl alcohol)/thiophene (0.076 mol) systems (MPT76) and the MPT152 systems, respectively. For the MPT76 systems, we observed the fiber morphologies for the complexes; transformations from fibers to a silk-like morphology occurred after increasing the amount of added thiophene to 0.152 mol. Further physical differences existed between these two systems. For instance, the silk-like morphology fabricated from the CuPT152 system exhibited fluorescence under polarized-light OM (Figure 10), whereas the fiber morphology fabricated from the CuPT76 system exhibited little of this behavior. The fluorescence emission derived from the great amount of the

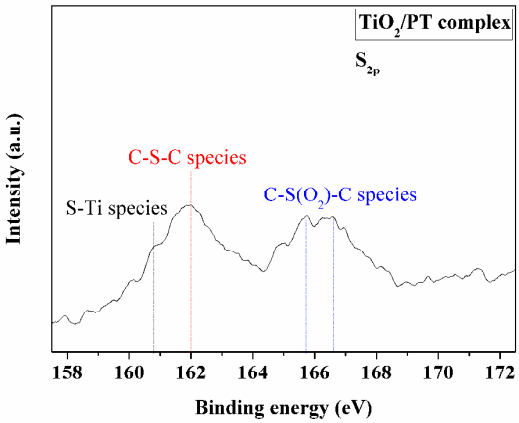

Figure 11: The XPS result of TiO2/PT complex.

conjugated polymer PT in the CuO/PTs complex. Thus, the morphology and structure of the metal oxide/PTs complex could be transformed by varying the content of thiophene in the reaction medium; these changes also affected the conductivity and absorption. Thus, when the signal in the XRD spectrum for the (100) plane at values of 2θ of 2.3–6.3° became flat in the presence of the PTs, the morphology of the complex became silk-like, due to the lower compatibility between the metallic composite and the PTs. In other words, the structure of the complex was disrupted in the presence of a greater amount of PTs. Hence, good stacking of the lattices of the metallic composites was not compatible with the PT chains. Table 1 summarizes the morphology with different amounts of thiophene monomer and metal precursors.

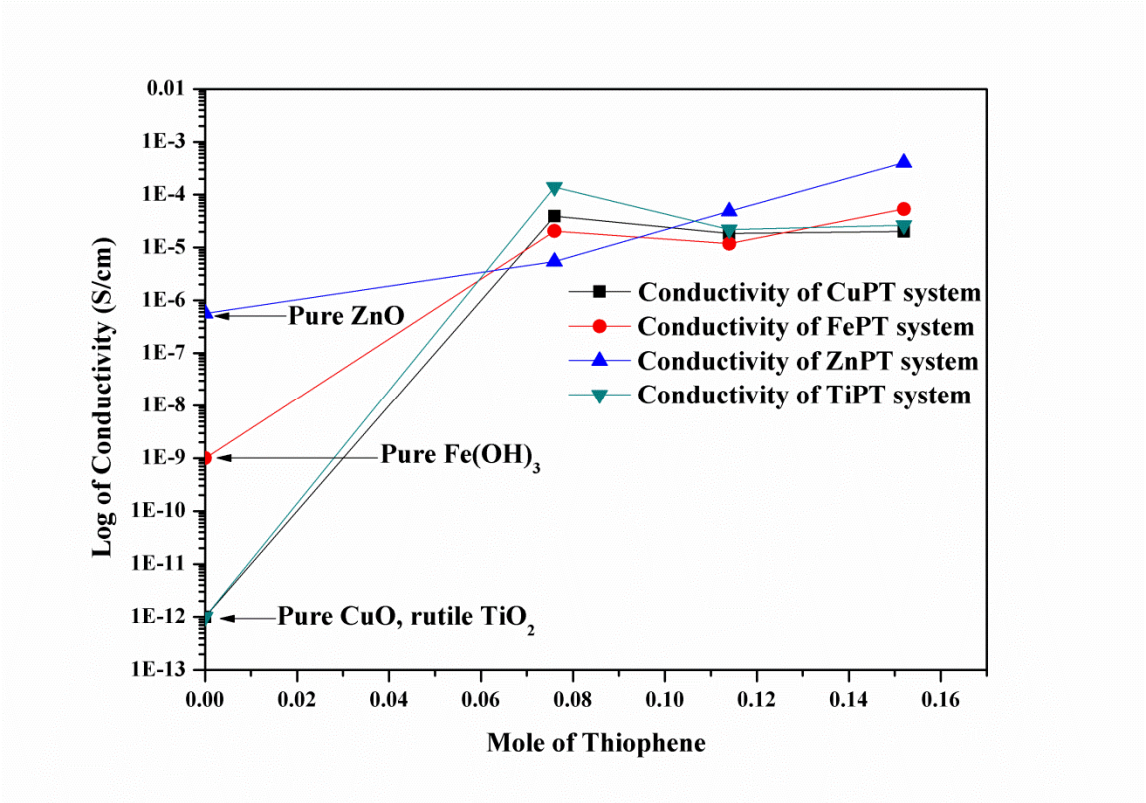

Figure 12: Conductivity curves of the metallic composite/PT complexes fabricated from the MPT system.

Table 1: Morphology change with different amounts of thiophene monomer and metal precursors

Amount of thiophene monomer	Metal precursor	Morphology
0.076 mole	$CuCl_2$	Fiber
0.114 mole	$CuCl_2$	Fiber
0.152 mole	$CuCl_2$	Silk
0.076 mole	$FeCl_3$	Fiber
0.114 mole	$FeCl_3$	Fiber (needle)
0.152 mole	$FeCl_3$	Silk
0.076 mole	$ZnCl_2$	Rod
0.114 mole	$ZnCl_2$	Rod, Fiber
0.152 mole	$ZnCl_2$	Silk
0.076 mole	$TiCl_3$	Rod
0.114 mole	$TiCl_3$	Rod, Fiber
0.152 mole	$TiCl_3$	Silk

Here, we also measured the critical bonding C-S-C,[30] C-S(O2)-C, and S-Metal species by XPS as shown in Figure 11. At this Figure, the C-S-C and C-S(O_2)-C species respectively were confirmed in the 161.5-163 eV and 164.5-167.5 eV. Moreover, the most important bonding representing the S-Metal chelation as S-Ti could be shown in the region 160-161 eV, and this binding energy region regularly used to symbol the chelating relation of thio-metal as thio-tungsten.[31]

Conductivity of the complexes

Figure 12 displays the conductivity curves of the metal oxide/PTs fabricated from the MPT systems. We observed low conductivity (2.7×10^{-12} S/cm) for the p-type semiconductor CuO in the absence of the PT. In contrast, the CuO/PTs complex fabricated from the CuPT76 system exhibited a conductivity of 3.9×10^{-5} S/cm. Rutile TiO_2, which has a conductivity of 1×10^{-12} S/cm, is a familiar p-type semiconductor; we measured a conductivity of 1.4×10^{-4} S/cm for the TiO_2/PTs complex fabricated from the TiPT76 system. Although metal oxides have high resistivity (e.g., 1.8×10^6 Ω cm for ZnO), we observed increased conductivity (to5.5×10^{-6} S/cm) for the fiber morphology of the ZnO/PTs complex fabricated from the ZnPT76 system. Furthermore, both the polymers and the metal hydroxides can be considered, in isolation, as insulating materials. For example, $Fe(OH)_3$ and PTs possess conductivities of 1×10^{-9} and 1×10^{-6} S/cm, respectively. Although the conductivities of PTs are typically higher than those other conjugated polymers, they are much lower than that of our $Fe(OH)_3$/PTs complex. Thus, the fiber morphology decreased the resistivity significantly, primarily because the fiber morphology could supply electrons for transmission and excited over a short distance. It corresponds to the fiber structure supplied a well conductive route for hole and electrons, the electrons could waste a little energy to transfer in intermolecular; however, more loss energies would occur in discontinuous particle structure. Therefore, such the other normal work as electro spun, the polymeric fiber materials can advance interlinking of the noble

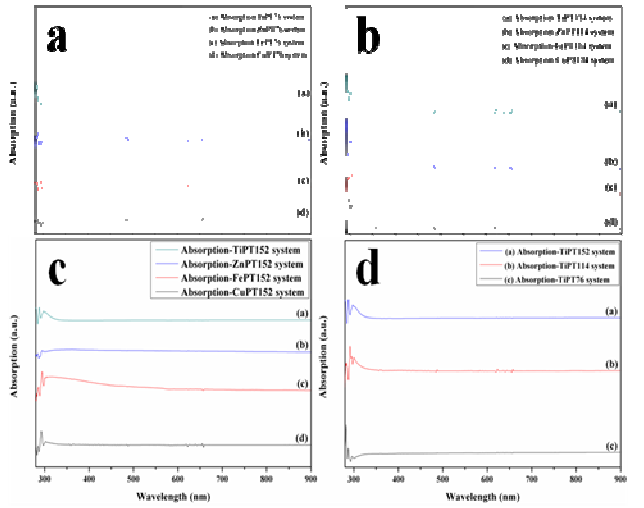

Figure 13: Absorption spectra of the products fabricated from the (a) MPT76, (b) MPT114, (c) MPT152, and (d) TiPT systems.

metal particles for well conductive property. The conductivities of our metal composite/PT systems changed from high to low, however, upon increasing the amount of thiophene in the reaction mixtures—the result of changing the morphology in the metal composite/PT complex from fibers to silk-like structures. Accordingly, the electrons could not undergo efficient conduction. On the other hand, the mechanism of conduction for a semiconductor requires the generation of electron/hole pairs. Therefore, its conductivity is less than that of a metal because the electrons of the valence band require sufficient energy to transition into a conductive band. In otherwise, the broken of metal structure would exist in the excessive PT system; that represented the polycrystalline and more grain-boundaries structure restricted the transmission of electron. Compare to singlecrystalline metal oxide structure, the electrons could be unrestricted jump in intermolecular. The results of broken metal oxide structure have proved by XRD and Fig. 1(b). The literature states that highly regular PTs structures can form when its polymerization is restricted at low temperatures. Good π–π stacking exists in such PT structures, resulting in good conductivity. Although the conductivities of our metallic composite/PT systems tended to be low after transformation of their morphologies from fiber to silk-like structures, the conductivities of these complexes remained in the range from 10^{-5} to 10^{-4} S/cm because they possessed firm structures with good transmission factors for electrons.

Photophysical properties of metallic composite/PTs

Figures 13(a)–(c) display the UV–Vis absorption spectra of the metallic composite/PT complexes; the energy level of each complex was located in the range from 3.75 to 4.27 eV. The absorption of a PT typically occurs at a wavelength range of 431-450 nm,[32] but this absorption disappears in a complex, such as a TiO_2/PT system, because of the existence of energy transfer. In other words, the electrons in the electronic band of the metallic composite can jump to lowest unoccupied molecular orbital (LUMO) of a PT after excitation under UV irradiation. On the other hand, the phenomenon in which an electron in the valence band of the metallic composite can transfer into the lowest unoccupied molecular orbital of the PT over a short distance will enhance the conductive properties of a complex. As a result, the energy level of the our complexes were greater than those of the metal oxide or PT alone, due to transitions in the morphologies and energy levels. For example, Figure 13(d) presents the spectra of the TiO_2/PT complexes fabricated from the TiPT76, TiPT114, and TiPT152 systems. A blue-shift in the absorption wavelength occurred as the morphology transformed from a silk-like to a fiber structure. The electrons transferred from the conductive band of the metallic composite to the LUMO of the PTs after passing its valence band; hence, the electrons required more energy to overcome the energy levels.[33,34]

Conclusion

By applying a facile and novel technique, a quenching method, we have fabricated metallic composite/PT complexes exhibiting fiber morphologies and excellent conductivities. High affinity between a metallic composite and a PT affected the ratios of nucleation and growth, resulting in the complexes having the fiber morphology. These complexes exhibited conductivities, ranging from 10^{-5} to 10^{-3} S/cm, that were higher than those of the pure metallic composites or of PTs because the fiber morphologies enhanced the conduction of electrons. In addition, the complexes possessed the properties of colloids, suggesting that they could be coated on most types of substrates, including glass; moreover, these complexes could applied in large-scale gas sensor with specific flexibility and porosity, even could simplified the transporting layers with solar cell preparation.

Acknowledgments

We than Professor Cheng Chien Lin and his group at National Chiao Tung University for XRD analysis as well as the Ministry of Science and Technology, Republic of China, for financial support (MOST 100-2221-E-110-029-MY3 and MOST 102-2221-E-110-008-MY3).

References

1. D. I. Suh, C. C. Byeon, and C. L. Lee, *Appl. Surf. Sci.* 2010, **257**, 1454–1456.
2. G. Jimenez-Cadena, E. Comini, M. Ferroni, A. Vomiero, and G. Sberveglieri, *Mater. Chem. Phys.* 2010, **124**, 694–698.
3. T. T. Tseng, and W. J. Tseng, *Ceram. Int.* 2009, **35**, 2837–2844.
4. S. W. Kuo, Y. C. Chung, K. U. Jeogn, and F. C. Chang, *J. Phys. Chem. C* 2008, **112**, 16470-16477.
5. J. Gong, L. Luo, S. H. Yu, H. Qian, and L. Fei, *J. Mater. Chem.* 2006, **16**, 101–105.
6. Y. C. Lin, C. H. Chen, L. Y. Chen, S. C. Hsu, and S. Qia, *RSC Adv.* 2014, **4**, 45419-45424.
7. K. Amikura, T. Kimura, M. Hamada, N. Yokoyama, J. Miyazaki, and Y. Yamada, *Appl. Surf. Sci.* 2008, **254**, 6976–6982.
8. Z. Paszti, Z. E. Horvath, G. Peto, A. Karacs, and L. Guczi, *Appl. Surf. Sci.* 1997, **109**, 67–73.
9. V. Amendola, and M. Meneghetti, *J. Mater. Chem.* 2007, **17**, 4705–4710.
10. F. Lin, J. Yang, S. H. Lu, K. Y. Niu, Y. Liu, J. Sun, and X. W. Du, *J. Mater. Chem.* 2010, **20**, 1103–1106.
11. X. Zheng, L. Zhu, X. Wang, A. Yan, and Y. Xie, *J. Cryst. Growth* 2004, **260**, 255–262.
12. Z. Wang, Z. Zhao, and J. Qiu, *J. Phys. Chem. Solids* 2008, 69, 1296-1300.
13. W. M. Cheng, C. C. Wang, and C. Y. Chen, *J. Colloid Interface Sci.* 2010, 348, 49–56.
14. L. Tang, B. Zhou, J. Zhao, X. Lv, F. Sun, and Z. Wang, *Colloids Surf., A* 2009, **332**, 43-49.
15. L. Wu, Y. Wu, H. Wei, Y. Shi, and C. Hu, *Mater. Lett.* 2004, **58**, 2700–2703.
16. J. Zhao, Z. G. Jin, T. Li, and X. X. Liu, *J. Eur. Ceram. Soc.*

2006, **26**, 2769-2775.
17. Q. R. Hu, S. L. Wang, Y. Zhang, and W. H. Tang, *J. Alloys Compd.* 2010, **491**, 707-711.
18. Y. Zhao, Y. Zhang, Y. Li, Z. He, and Z. Yan, *RSC Adv.* 2012, **2**, 11544-11551.
19. D. T. Nguyen, D. J. Kim, M. G. So, and K. S. Kim, *Adv. Powder Technol.* 2010, **21**, 111–118.
20. Y. Mikhlin, A. Karacharov, M. Likhatski, T. Podlipskaya, Y. Zubavichus, A. Veligzhanin, V. Zaikovski, J *J. Colloid Interface Sci.* 2011, **362**, 330–336.
21. J. Zou, J. Jiang, L. Huang, H. Jiang, and K. Huang, *Solid State Sci.* 2011, **13**, 1261-1267.
22. J. Lu, Z. Ye, J. Huang, L. Wang, and B. Zhao, *Appl. Surf. Sci.* 2003, **207**, 295–299.
23. F. H. Lu, M. M. Mohamed, T. F. Liu, F. C. Chang, C. G. Chao, and S. W. Kuo, *J. Mater. Chem. C* 2014, **2**, 6111-6118.
24. F. Bayansal, H. A. Çetinkara, S. Kahraman, H. M. Çakmak, and H. S. Guder, *Ceram. Int.* 2012, **38**, 1859–1866.
25. T. A. Chen, X. Wu, and R. D. Rieke, *J. Am. Chem. Soc.* 1995, **117**, 233-244.
26. P. T. Wu, H. Xin, F. S. Kim, G. Ren, and S. A. Jenekhe, *Macromolecules* 2009, **42**, 8817–8826.
27. M. A. Ibrahim, B. G. Lee, N. G. Park, J. R. Pugh, D. D. Eberl, and A. J. Frank, *Synth. Met.* 1999, **105**, 35–42.
28. Y. Wang, X. Li, N. Wang, X. Quan, and Y. Chen, *Sep. Purif. Technol.* 2008, **62**, 727-732.
29. C. C. Chen, P. Liu, C. H. Lu, *Chem. Eng. J.* 2008, **144**, 509–513.
30. S. Jayaraman, P. S. Kumar, D. Mangalaraj, D. Rajarathnam, S. Ramakrishna, M. P. Srinivasan, *RSC Adv.*, 2014, **4**, 11288–11294.
31. S. Bai, K. Zhang, J. Sun, D. Zhang, R. Luo, D. Li, C. Liu, *Sens. Actuators B*, 2014, **197**, 142-148.
32. L. Zhai, and R. D. McCullough, *J. Mater. Chem.* 2004, **14**, 141–143.
33. E. Katsia, N. Huby, G. Tallarida, B. Kutrzeba-Kotowska, M. Perego, S. Ferrari, F. C. Krebs, E. Guziewicz, M. Godlewski, V. Osinniy, and G. Luka, *Appl. Phys. Lett.* 2009, **94**, 143501.
34. K. Noori, and F. Giustino, *Adv. Funct. Mater.* 2012, **22**, 5089–5095.

A Graphic Content

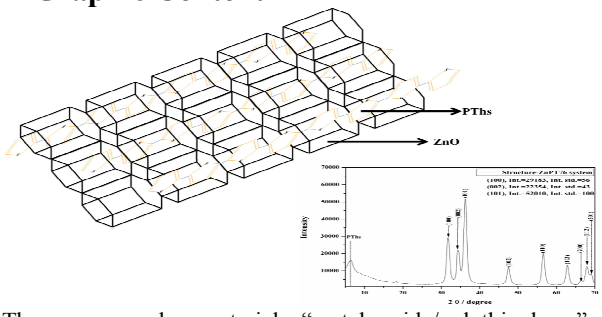

The new complex materials "metal oxide/polythiophene" was synthesized by one-pot quenching method, and the well conductivity (~10^{-3} S/cm of pure metal oxide and polythiophene) have specific luminescence property, and fiber morphology were performance in these complexes